Nondestructive Bridge Deck Testing with Air-Coupled Impact-Echo and Infrared Thermography

Seong-Hoon Kee[1]; Taekeun Oh[2]; John S. Popovics, M.ASCE[3]; Ralf W. Arndt[4]; and Jinying Zhu, A.M.ASCE[5]

Abstract: Two different nondestructive test (NDT) methods, air-coupled impact-echo (IE) and infrared (IR) thermography are evaluated on a full-scale simulated reinforced concrete bridge deck containing simulated delamination and cracking defects. The IE data are presented as two-dimensional frequency maps and spectral B-scan lines. The IR data are presented as temperature maps on the concrete surface. The lateral boundaries of the detected delaminations are also indicated in the images. The results obtained from each of the individual NDT methods show reasonably good agreement with most of the actual defects. The advantages and limitations of each method to characterize defects are discussed. The consistency and sensitivity of each method are also investigated. Finally, a simple data fusion technique is proposed to improve effectiveness of the individual test data. The findings from this study demonstrate that the combination of air-coupled IE and IR thermography tests is a practical option for consistent and rapid in situ evaluation of reinforced concrete bridge decks. **DOI: 10.1061/(ASCE)BE.1943-5592.0000350.**

CE Database subject headings: Nondestructive tests; Delaminating; Concrete bridges; Bridge decks; Thermal factors.

Author keywords: Nondestructive test; Delamination; Air-coupled impact echo; Infrared thermography; Data fusion; Concrete bridge deck.

Introduction and Motivation

Concrete in civil infrastructure systems is susceptible to deterioration caused by various mechanisms. Reinforced concrete (RC) bridge decks are especially susceptible to early deterioration, and often must be repaired or replaced several times throughout the lifetime of the bridge structure. In particular, chloride-based deicing agents applied in winter seasons have contributed significantly to deterioration of RC bridge decks. The deck deterioration manifests as various defects (e.g., cracking, scaling, and delamination) with varying severity. The most serious problem affecting the service life of RC bridge decks is the formation of a delamination, which is a thin cracked area that lies directly above the steel reinforcement mat within the deck. The presence of delamination may cause further deterioration (e.g., generating vertical cracks and spalling) that disrupts the operation of the structure, and in some cases threatens the safety of the public.

Infrastructure management agencies in the United States dedicate a sizable portion of their construction budget, in excess of $2.0 billion annually, to the maintenance of concrete bridge decks (Koch et al. 2002). To maximize the working efficiency with limited sources, maintenance actions are generally prioritized based on the expected current condition of a structure. In most cases deck condition evaluation relies primarily on visual examination and sounding (chain drag and hammer tap) with some limited destructive tests; for example, core extractions. However, visual inspections provide only superficial information, and the results depend on the experience of the inspectors (Moore et al. 2001). Moreover, visual inspections are not effective to identify delamination hidden in concrete bridge decks. The sounding method is subjective in nature, and requires experienced inspectors to acquire accurate results. Destructive tests such as core extraction may provide detailed information of the concrete condition; however, they are labor intensive and time consuming and cannot be applied ubiquitously over large areas of the structure. Thus, nondestructive test (NDT) methods, which can be applied rapidly and ubiquitously across the bridge deck structure, find much utility. Judicious application of NDT methods can help determine the optimum timing of inspections and rehabilitations to minimize the total cost in maintenance and disruption of service. Several established NDT methods are normally applied to bridge decks, including impact-echo (IE), infrared (IR) thermography, ground penetrating radar (GPR), and sounding (chain drag). Each of these methods has certain advantages and disadvantages (ACI 1998). The principal advantage of IE is its high sensitivity to the presence of internal delamination and its fundamental basis, which is rooted in the mechanical behavior of the concrete deck material. The principal advantage of IR is that it provides a full-field image of the bridge deck surface, which under ideal testing conditions provides an accurate description of the near-surface delamination location, areal size, and shape.

Background

The purpose of this study is to improve NDT methods for evaluating RC bridge decks. Two of the more promising NDT methods for RC

[1]Postdoctoral Research Associate, Center for Advanced Infrastructure and Transportation, Rutgers, State Univ. of New Jersey, 100 Brett Rd., Piscataway, NJ 08854-8058. E-mail: seonghoonkee@utexas.edu

[2]Graduate Research Assistant, Dept. of Civil and Environmental Engineering, Univ. of Illinois at Urbana–Champaign, 205 N. Mathews Ave., MC-250, Urbana, IL 61801. E-mail: toh5@illinois.edu

[3]Associate Professor, Dept. of Civil and Environmental Engineering, Univ. of Illinois at Urbana–Champaign, 205 N. Mathews Ave., MC-250, Urbana, IL 61801. E-mail: johnpop@illinois.edu

[4]Postdoctoral Research Associate, Center for Advanced Infrastructure and Transportation, Rutgers, State Univ. of New Jersey, 100 Brett Rd., Piscataway, NJ 08854-8058. E-mail: ralf.arndt@rutgers.edu

[5]Assistant Professor, Dept. of Civil, Architectural, and Environmental Engineering, Univ. of Texas, Austin TX 78712-0273 (corresponding author). E-mail: jyzhu@mail.utexas.edu

Note. This manuscript was submitted on June 27, 2011; approved on November 30, 2011; published online on December 2, 2011. Discussion period open until April 1, 2013; separate discussions must be submitted for individual papers. This paper is part of the ***Journal of Bridge Engineering***, Vol. 17, No. 6, November 1, 2012. ©ASCE, ISSN 1084-0702/2012/6-928–939/$25.00.

bridge decks are studied here, IE and IR thermography. The writers deploy the IE tests using an air-coupled sensing configuration, which negates some of the disadvantages of the traditional IE method, and attempt to find improved NDT performance through simple data fusion of the two techniques. The concept of the data fusion is based on the following: (1) collecting data from independent NDT methods; (2) extracting the most reliable results from each data set; and (3) merging those results into one set of result data. A brief introduction to each NDT method is provided.

Impact-Echo NDT Method

IE is a widely used NDT method, which has been demonstrated to be effective in detecting delaminations in bare (without asphalt overlay) concrete structures (Sansalone 1996; Tawhed and Gassman 2002; Zhu and Popovics 2007). IE is a mechanical-wave method based on the transient vibration response of a platelike structure subjected to mechanical impact. The mechanical impact generates body waves (P waves, or longitudinal waves, and S waves, or transverse waves), and surface guided waves (e.g., Rayleigh surface waves) that propagate within the solid material. The multiply reflected and mode-converted body waves eventually set up sets of infinite vibration resonance modes within the solid material (Tolstoy and Usdin 1953). The transient time response of the solid structure is measured with a contact sensor (e.g., displacement sensor or accelerometer) mounted on the surface close to the impact source. The Fourier transform (amplitude spectrum) of the time signal will show maxima (peaks) at certain frequencies, which represent particular resonant modes. Two sets of vibration modes are relevant to this study, the thickness stretch modes and the flexural drum modes. The thickness stretch mode family normally dominates the spectral response of a platelike structure that does not contain any near-surface defects. In that case, the frequency of the fundamental thickness stretch mode (also called the, IE frequency: f_{IE}) can be related to the thickness of the plate. Knowing the P-wave velocity C_p of concrete, the plate thickness H is related to the IE frequency f_{IE} by

$$H = \beta \frac{C_p}{2 f_{IE}} \tag{1}$$

where β = correction factor ranging from 0.945 to 0.957 for the normal range of concrete (Gibson and Popovics 2005). The correction factor is based on elastodynamic effects related to a S_1 Lamb wave mode with zero group velocity, which depends on the Poisson's ratio. The thickness stretch mode may also dominate the spectral response when the test is carried out over a relatively deep defect or delamination. However, the flexural modes tend to dominate the spectral response when a test is carried out over a shallow (near-surface) defect or delamination. These modes normally have much lower frequency than the stretch modes. Unfortunately, a simple analytical expression that relates the fundamental flexural frequency to the defect depth has not yet been established because this frequency value depends on the plate geometry, shape, and boundary condition. Despite this problem, IE test data provide valuable information about the presence of delaminations in concrete plates; areas that show a dominant response frequency with a relatively low value are likely located above the shallow delamination defects, although the depth of the defect cannot be directly estimated.

However, in practice some infrastructure engineers are reluctant to apply IE to RC bridge decks because of the relatively slow testing rate and inconsistent coupling conditions that are encountered when conventional contact sensors are used. An effective solution to this problem is the use of contactless sensors. Both laser vibrometers and air-coupled acoustic sensors (microphones) have been used for this purpose. Laser vibrometers must overcome many practical challenges such as high equipment cost, the inability to detect waves on rough concrete surfaces, and varying ambient light conditions before they can be widely deployed for this purpose. In contrast, air-coupled sensors have been successfully used to measure leaky surface waves (Zhu and Popovics 2005; Ryden et al. 2008; Kee and Zhu 2010; In et al. 2009) and Lamb waves (Zhu and Popovics 2007; Holland and Chimenti 2003) in concrete and other solid materials. Recently, air-coupled sensors were demonstrated to be working well in an IE test setup for evaluating various defects (delaminations with various sizes and depths and volumetric defects) in a concrete slab in the laboratory (Zhu and Popovics 2007). However, thus far air-coupled IE tests have been limited to laboratory specimens.

Infrared Thermography NDT Method

IR thermography makes use of temperature-dependent electromagnetic surface radiation in the IR wavelength to detect subsurface defects. The application of IR thermography is divided into two categories, passive and active, depending on the heat sources employed. In passive thermography the distribution of surface temperature and its relevant heat sources are only defined by the function of the component itself and its natural environment (Geyer and Arndt 1993), and usually only one data set at a certain time is taken. The heat flow through the component can be described by the steady-state Fourier equation

$$0 \approx \left\{ \frac{\partial^2 \phi}{\partial x^2} + \frac{\partial^2 \phi}{\partial y^2} + \frac{\partial^2 \phi}{\partial z^2} \right\} \tag{2}$$

where ϕ = temperature and x, y, and z = spatial coordinates. In active thermography a temperature gradient is generated by the user, and the subsequent compensation process monitored over a relevant period of time allows quantitative size and depth characterization of defects. The heat flow is ruled by the Fourier equation for the transient state

$$c \cdot \rho \frac{\partial \phi}{\partial t} = w + \lambda \cdot \left\{ \frac{\partial^2 \phi}{\partial x^2} + \frac{\partial^2 \phi}{\partial y^2} + \frac{\partial^2 \phi}{\partial z^2} \right\} \tag{3}$$

where c = specific heat capacity, ρ = density, w = rate of energy generation in the medium, and λ = thermal conductivity.

The principal advantage of passive IR thermography is that it allows global visualization of the temperature distribution on surfaces with high accuracy and speed without defect depth information. On the other hand, active thermography can provide depth information and is less affected by boundary conditions. However, it is much more time and cost intensive. A form of passive IR thermography has been successfully applied in the detection of delaminations in bridge decks by taking advantage of the cyclic solar energy that illuminates the deck. In 1988 this method was standardized under ASTM D4788 (ASTM 1997). In this study, a modified methodology is used that makes use of nightly cooling effects and by making periodic measurements. Although a form of passive thermography is applied, the heat flow can be described by the unsteady-state Fourier Eq. (3).

Experimental Program

Specimen Preparation

A simulated bridge deck section was prepared at the University of Texas at El Paso, as part of a research project to compare NDT technologies for concrete bridge deck deterioration detection. The

J. Bridge Eng. 2012.17:928-939.

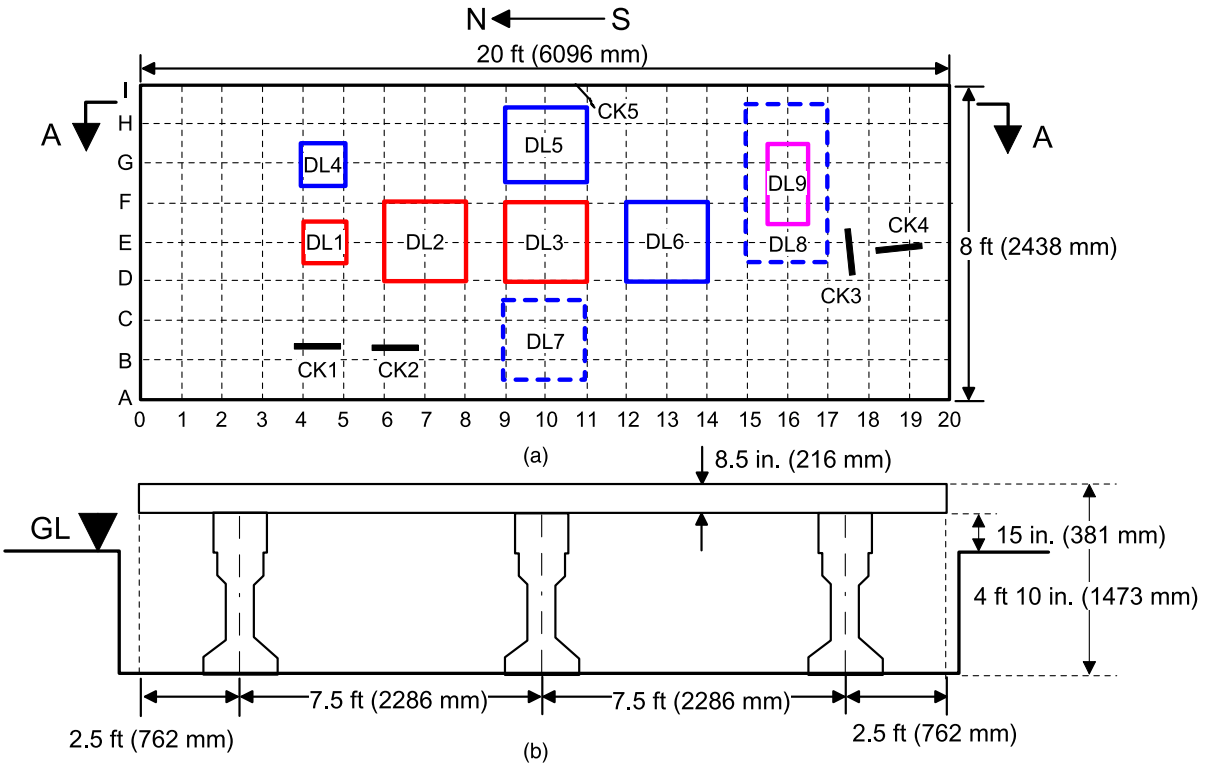

Fig. 1. RC bridge deck specimen: (a) plan view of the specimen showing the location of the defects and the test grid designation (detailed information is shown in Table 1); (b) section view (A-A) of the specimen [shallow delaminations are indicated by solid lines and deep delaminations are indicated by dashed lines; the nominal grid spacing is 0.305 m (1 ft) in both directions]

writers applied their respective NDT technologies at this test site. However, verification (by destructive means) of the actual size, location, and condition of the simulated defects within the deck was not allowed. The section consisted of a concrete deck and three supporting concrete beams as shown in Fig. 1. The concrete deck has length × width × depth dimensions of 6.09 m (20 ft) × 2.436 m (8 ft) × 0.216 m (8.5 in.), which is large enough to simulate a full-scale RC bridge section. In addition, the bridge deck slab was built with two mats of uncoated steel reinforcement at 60-mm (2.5-in.) and 150-mm (6-in.) depths, respectively. Each of the reinforcement mats consist of No. 5 steel bars spaced at 200 mm (8 in.) in the transverse direction and 250 mm (10 in.) in the longitudinal direction. A Texas Department of Transportation (TxDOT) Class S concrete mixture was used for the deck construction, which is broadly used in bridge deck construction by TxDOT. The mixture was designed to have minimum 28-day compressive strength of 28 MPa (4,000 psi). The deck slab was broom finished for a rough surface and water cured for 7 days after casting. The actual measured 28-day strength was higher than 35 MPa (5,000 psi).

The simulated deck was designed to contain fabricated delaminations (various materials were used to simulate the delamination defects) by inserting foam pieces or polyester fabric with various sizes and at two different depths, shallow delaminations at 60-mm (2.5-in.) depth and deep delaminations at 150-mm (6-in.) depth. Simulated vertical cracks were also built in the deck by inserting cardboard pieces before casting concrete. Fig. 1(a) shows an overview of the horizontal distribution of these defects as built in the deck slab. Detailed information about the defects is provided in Table 1. In Fig. 1(a) and Table 1, DL denotes delamination and CK denotes vertical crack. In addition, a natural vertical crack was observed in the deck slab two weeks after construction around Grid Point 11-I.

Table 1. Detailed Information of Preplaced Delamination Defects within the Concrete Specimen

	Size		Depth		
Defect code	cm	in.	cm	in.	Material/remark
DL1	30.5 × 30.5	12 ×12	6.35	2.5	Soft and high-strength
DL2, DL3	61 × 30.5	24 × 24	6.35	2.5	thin foam [1 mm (39 mil)]
DL4	30.5 × 30.5	12 × 12	6.35	2.5	Soft and high-strength
DL5, DL6	61 × 61	24 × 24	6.35	2.5	thick foam [2 mm (78 mil)]
DL7	61 × 61	24 × 24	15.24	6	Soft and high-strength
DL8	30.5 × 61	24 × 48	15.24	6	thin foam [1 mm (39 mil)]
DL9	30.5 × 61	12 × 24	6.35	2.5	Very thin soft polyester fabric [0.3 mm (12 mil)]

Air-Coupled IE Equipment

Two prototype air-coupled IE testing equipment sets were developed separately by the University of Illinois and the University of Texas. The air-coupled IE test equipment developed at the University of Illinois (referred to as Prototype A) is shown in Fig. 2(a). Prototype A contains five unshielded dynamic (unpowered) microphones (Model: SM58, Shure, Inc.) that are mounted onto a small rolling cart with a horizontal mounting frame. The microphone had a flat frequency response from 50 Hz to 15 kHz, with a nominal sensitivity of 1.85 mV/Pa at 1 kHz. A 18-mm-diameter (3/4-in.-diameter) steel ball was used as the impact source. The frame

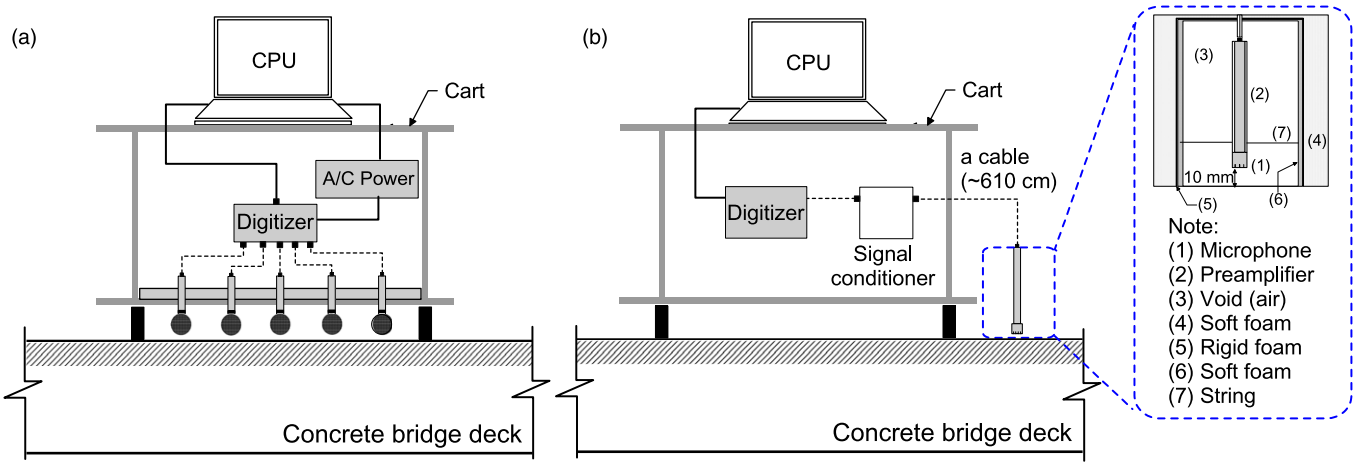

Fig. 2. Air-coupled IE testing equipment sets developed by the (a) University of Illinois (Prototype A) and (b) University of Texas (Prototype B), including detail of the sound insulation for the microphone

positioned the microphones at a 150-mm (6-in.) transverse spacing and held them about 12 mm (1/2 in.) above the surface of the deck. The microphones were connected to a multichannel analog-to-digital (A/D) converter (NI-USB 6259) with an aggregate sampling frequency of 1 MHz and 4 ms duration time. The digitized data were then fed to a laptop computer that runs a data acquisition program under the *MATLAB* platform. A self-contained AC current supply unit powered the computer and A/D converter. All testing equipment was carried on the cart, which could be easily moved along the deck surface. Two people were needed to operate Prototype A, one to operate the data acquisition equipment and the other to apply impact events at each test location.

The air-coupled test equipment developed by the University of Texas (referred to as Prototype B) is shown in Fig. 2(b). The configuration of Prototype B was similar to Prototype A. However, there were several important differences that affected the overall performance of the equipment. A high-sensitivity broad bandwidth air-coupled sensor (Model: PCB 377B01) was used in Prototype B. That sensor had a small size [diameter of 6.3 mm (0.25 in.)], broad frequency range (4−80 kHz at ± 2 dB), and high sensitivity (4 mV/Pa). The microphone was shielded by a sound insulation device shown in Fig. 2(b) to reduce the effects of direct acoustic waves and ambient noise (Kee 2011). A steel ball with a diameter of 13 mm (0.5 in.) was used as an impact source. The deck slab vibrations set up by the impact source were measured by the microphone and amplified by a battery powered signal conditioner. The output signals were digitized at a sampling frequency of 500 kHz using an NI-USB 5133 oscilloscope, which is bus-powered and portable. Each dynamic signal was collected for a duration of 10 ms. The acquired signals were transferred to and stored in a laptop computer. The data acquisition and saving procedure were controlled by a *LabVIEW*-based computer program. All equipment was carried on a cart and operated by two people, one for data collection and the other for moving the sensor and applying the impact source.

Testing Procedure and Scheme for Air-Coupled IE

The two testing prototypes were independently used to perform acoustic scanning of the bridge deck specimen. Prototype A [see Fig. 2(a)] was first used to evaluate the test specimen with five sensors across a 60-cm (2-ft) transverse span as the cart traveled longitudinally along the deck. Thus, the entire width of the test region was covered in three longitudinal scans as shown in Fig. 3(a). At each test point, an impact event was manually applied to the surface of the concrete deck with a hardened 18-mm-diameter (3/4-in.-diameter) steel sphere mounted on a wire. The dynamic response was measured by a microphone nearby the impact and stored in the laptop computer. Then, the signal from the next test point was collected and saved in consecutive order. The process was continued until data from all five microphones on the mounting rack were collected, after which the line of microphones were moved longitudinally to the next testing location using the cart. The cart was moved longitudinally in increments of 150 mm. All of the data scans on the concrete deck represent a total of 455 test points over 9.45 m^2 (102 ft^2). The tests were carried out in a natural outdoor ambient environment (passing vehicles, wind, talking by test operators), which is representative of a test carried out on a bridge deck without any sort of noise shielding or suppression technology. Scans along Lines E were carried out three separate times to have sets of repeated test data to check the consistency of the testing equipment.

Prototype B [shown in Fig. 2(b)] was independently used to conduct acoustic scanning of the test specimen with a single shielded microphone. The scanning started at Grid Point 1-A, and moved along transverse Grid Line 1 at an interval of 0.305 m (1 ft). The microphone was connected to the data acquisition equipment on a cart with a 6.09-m-long (20-ft-long) cable, which was long enough to cover the transverse line without moving the cart. The acoustic scanning was repeatedly performed column by column in the transverse direction as the cart moved longitudinally along Line E [see Fig. 3(b)]. All of the data scans on the concrete deck represent a total of 91 test points compared with 455 from Prototype A. In addition, three repeated scans were performed along Line E to check the consistency of the equipment.

IR Thermography Equipment and Application

The test specimen was also investigated by quasi-passive IR thermography using a commercially available uncooled microbolometer focal plane array IR camera (FLIR T400) (FLIR Systems 2011), which is sensitive in wavelengths of 7.5−13 μm (0.295−0.511 mil). The operation of the IR camera to measure the temperature distribution of the concrete surface is illustrated in Fig. 4. The data were processed using the *ThermaCAM QuickReport* software from FLIR. Afterward, the data were remapped (deskewed) into plan view using

J. Bridge Eng. 2012.17:928-939.

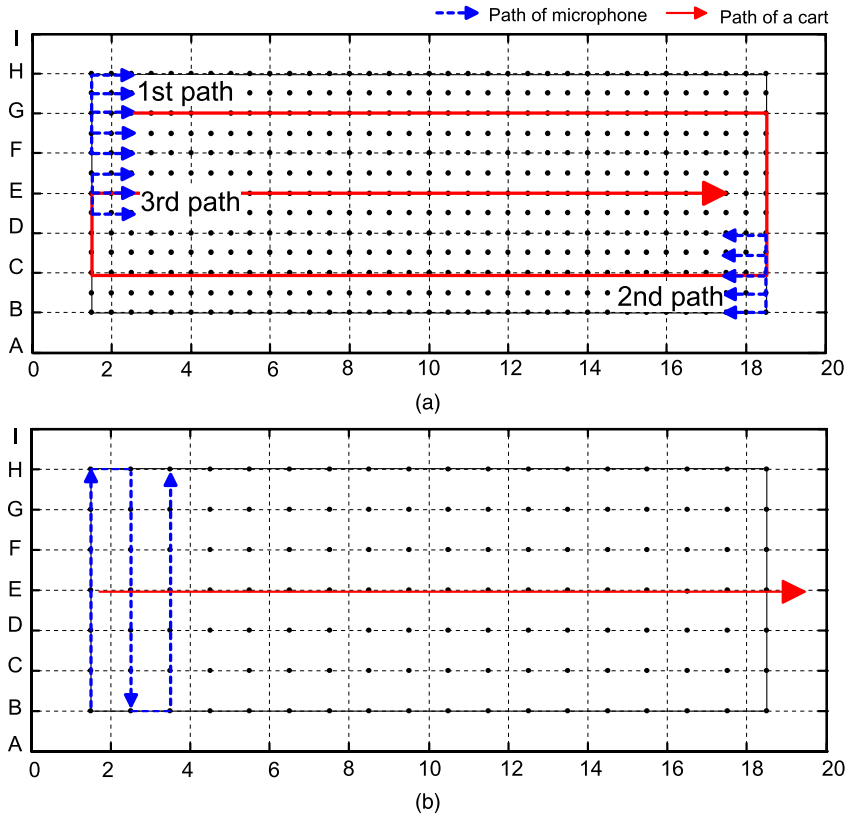

Fig. 3. Scanning procedure for air-coupled IE tests by the (a) research team from the University of Illinois and (b) University of Texas; black dots indicate test points, which are 0.15 m (6 in.) and 0.305 m (12 in.) in both directions in the tests done in (a) and (b), respectively

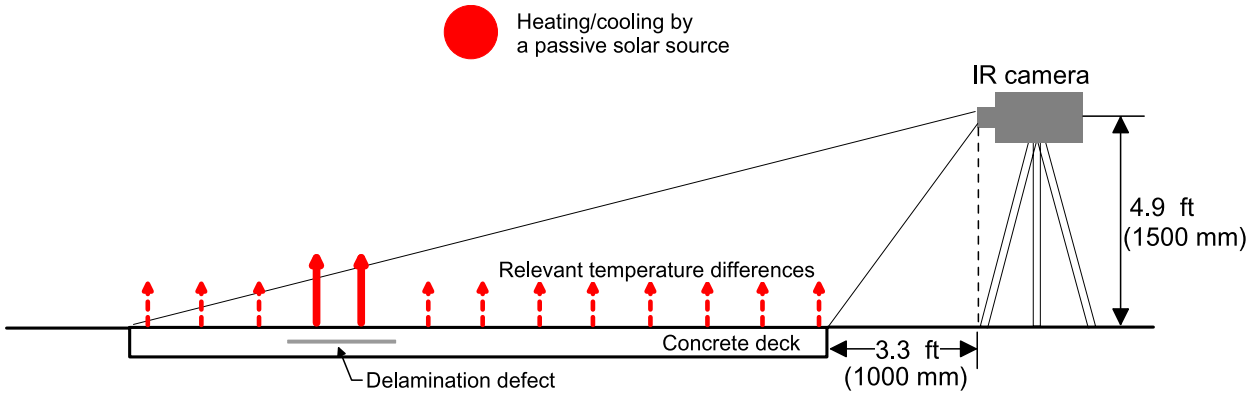

Fig. 4. Operation of the IR camera to measure the temperature distribution of the concrete surface

the image processing toolbox of *MATLAB*. The specific performance characteristics of the IR camera used in this study are summarized in Table 2. The optimal ambient conditions for quasi-passive IR data collection usually is about 4–6 h after sunrise, as described in ASTM D4788 (ASTM 1997). However, the first data set was taken about 40 min after sunrise (7:30 a.m.) to avoid shadowing effects caused by other groups operating on the specimen starting at 9 a.m., and furthermore to make use of the cooling effect that occurs overnight. Then, the IR data were collected periodically until 2:30 p.m. at intervals of about 1 h. At each measurement, a digital image and a fusion image were taken from each end of the test specimen (see Fig. 4).

Data Analysis

IE Method

The time domain signals measured by the microphones were converted to the frequency domain using the fast Fourier transform algorithm. Prototype A used the raw unprocessed time signal, while Prototype B applied a rectangular window to the raw time signals to eliminate contributions from the surface wave. All data analysis was performed by computer programs written by the writers.

Fig. 5 shows the typical signals in the time and frequency domains measured with the Prototype B testing equipment. Fig. 5(a)

J. Bridge Eng. 2012.17:928-939.

includes the time signals measured over the solid region at Grid Point 13.5-C, over shallow Delamination DL2 at 7.5-E, and over deep Delamination DL8 at 15.5-E, respectively. Fig. 5(b) shows the frequency spectra corresponding to the time signals shown in Fig 5(a). The frequency response from the solid region shows a dominant peak frequency around 9.0 kHz, which matches well with the full-thickness IE mode frequency calculated using Eq. (1). Deep delaminations generate an IE frequency that is higher than the full-thickness frequency (9.0 kHz). Shallow delaminations generate low-frequency responses with dominant frequencies between 1.5 and 2.5 kHz that are caused by the flexural drum vibration mode of the thin delaminated sections of concrete when tests are carried out over them.

IR Thermography Method

All bodies emit electromagnetic radiation according to their surface temperature and emissivity, which is the ability of a material to emit radiation at a certain wavelength. This radiation was measured by IR cameras and transferred into thermograms, which are images of the temperature distribution over the measured area (Maldague 2001). If the emissivity is known, IR cameras can calculate the surface temperature from the measured surface radiation quite accurately. However, for NDT applications the relative temperature contrast between sound areas and areas with defects is normally more pertinent than the temperature itself. Thus, typical practice—i.e., that described in ASTM D4788 (ASTM 1997)—considers an area as debonded or delaminated if the temperature difference with respect to an adjacent area is ± 0.5°K or °C (± 0.9°F); this recommendation assumes good testing conditions such as continuous sunshine for at least 3 h, clean and unspoiled surfaces, and a dry bridge for at least 24 h prior to testing. The standard allows a lower temperature contrast for nighttime measurements. Generally, deeper defects result in a smaller temperature contrast and appear subsequently in the heating/cooling cycle.

Table 2. Specifications of the IR Camera Used to Obtain IR Images

Item	Remark
Field of view	25° × 19°
Minimum focus distance	0.4 m (1.31 ft)
Thermal sensitivity[a]	0.05°C at + 30° (+ 86°F)/50 mK
Detector type	Focal plane array, uncooled microbolometer
IR resolution	320 × 240
Spectral range	7.5–13 μm (0.295–0.511 mil)
Digital zoom and pan/focus	1–8 × continuous/auto- and manual focus

[a]Noise equivalent temperature difference.

Results and Discussion

Frequency Map from Air-Coupled IE Tests

A frequency map is an image that presents the frequency at the highest spectral amplitude peak in the frequency domain signal at each test point across the tested surface. This presentation format has been shown to be useful for air-coupled IE data obtained from acoustic scanning (Zhu and Popovics 2007). The image is created using the contour plotting function in *MATLAB*. Figs. 6(a and b) are the frequency maps obtained from IE testing Prototypes A and B, respectively. The data points used to construct Figs. 6(a and b) were based on measurement test grid intervals of 150 mm (0.5 ft) and 300 mm (1 ft), respectively, as illustrated in Fig. 3. Consequently, a total of 455 and 91 test locations were measured using Prototypes A and B, respectively. In the plots, the frequency of the dominant spectral peak is indicated by grayscale, where dark areas indicate regions dominated by a low-frequency response, and light areas by a high-frequency response.

The resulting frequency maps were effective in identifying the presence and location of shallow delaminations in the concrete specimen. For the shallow delaminations with larger areal extent (i.e., DL2, DL3, DL5, and DL6), both frequency maps in Fig. 6 indicate low-frequency responses about 1.5 kHz, which are set up by the flexural drum modes. The shallow delaminations with smaller areal size (i.e., DL1 and DL4) are indicated in Fig. 6(a) as low-frequency regions with frequency around 2.5 kHz, which again correspond to the flexural vibration modes. However, the lower spatial resolution of the data of Prototype B [shown in Fig. 6(b)] hinders the ability to detect the shallow delaminations with small

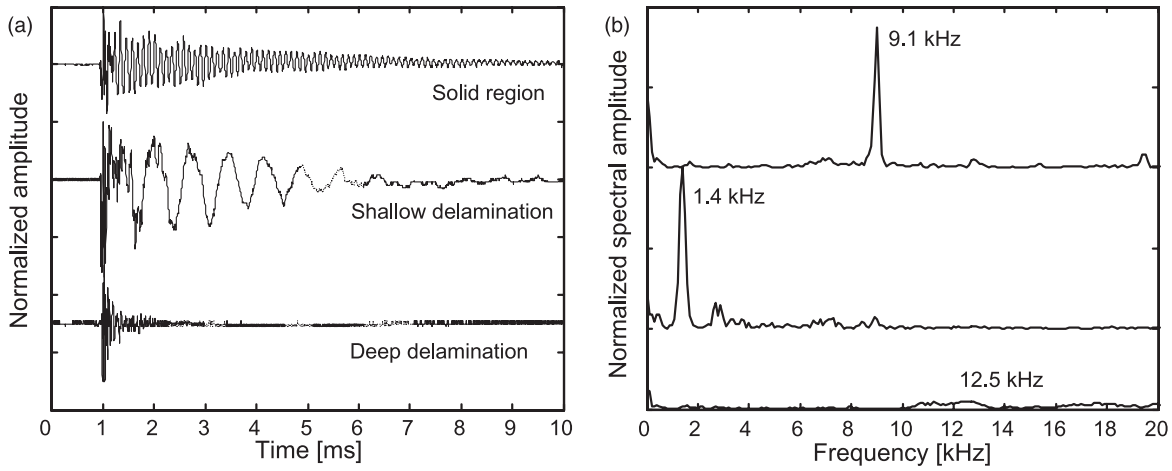

Fig. 5. Typical signals measured from the air-coupled sensors in various locations: (a) time signals measured over the solid region (Grid Point 12.5-C), over shallow delamination (Grid Point 7.5-E), and over deep delamination (Grid Point 15.5-E); (b) frequency spectra corresponding to the three time signals shown in (a)

J. Bridge Eng. 2012.17:928-939.

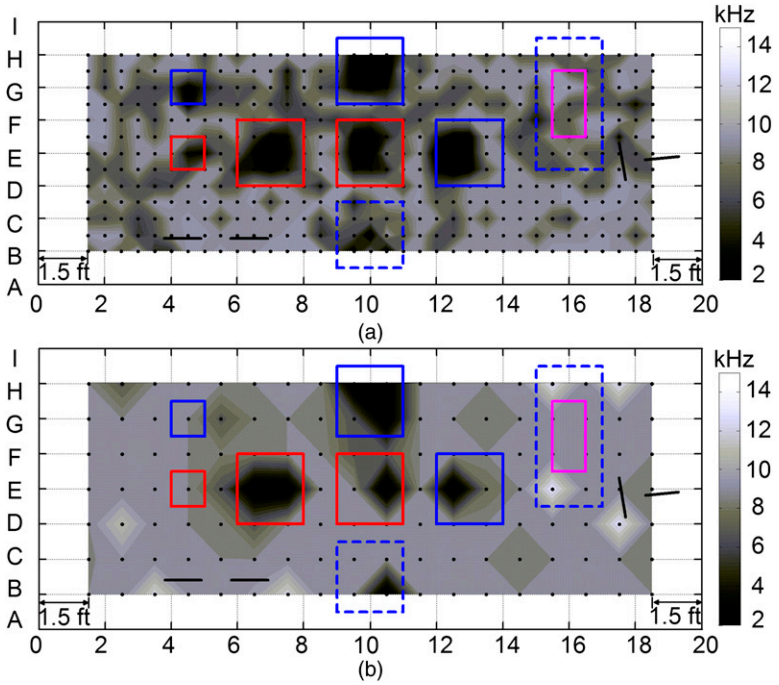

Fig. 6. Maps representing the frequency at the highest peak in the frequency spectrum from the IE tests: (a) data from the University of Illinois equipment (Prototype A); (b) data from the University of Texas equipment (Prototype B)

areal size; the peak frequency over those regions is only slightly lower than the IE frequency of the solid area. These results imply that the spatial resolution of the IE testing grid is important: finer testing grids enable detection of delaminations with smaller areal size. Based on previous numerical simulations and experimental work done by the writers, delamination defects smaller (in lateral dimension) than twice the test spacing have less chance of being detected. Furthermore, the frequency map image with finer test grid spacing provides better characterization of the areal extent of the delamination. None of the IE test data indicated the presence of shallow Delamination DL9; however; this result was unexpected. There are several possible reasons for this behavior: (1) the very thin width of the embedded delamination itself, (2) fabrication errors, and (3) inappropriate selection of material to simulate delamination. Previous studies indicate that the minimum air-filled delamination width that can be detected by IE is approximately 0.025 mm (0.984 mil) (Cheng and Sansalone 1995 a, b). The width of the embedded material that simulated air-filled Delamination DL9 was 0.3 mm (Table 1); thus, it appears that the delamination defect was not too thin to be detected by IE. The writers cannot exclude possible reasons (2) and (3) as the basis of this observed behavior.

For deep Delamination DL8 with a larger areal extent, data from Prototype B [Fig. 6(b)] showed a region of light area that corresponds to the frequency response around 12 kHz, which is close to the IE frequency of a deep delamination with a depth of 150 mm (6 in.) using Eq. (1). Data from Prototype A do not indicate the presence of deep Delamination DL8. On the other hand, the deep delamination with smaller areal extent, DL7, is indicated as a reduction in peak frequency with data from both prototypes; furthermore, this indication represents only a small portion of the actual defect area. It appears that the areal extent of a deep delamination must be sufficiently large compared with depth to set up dominant IE thickness stretch modes, enabling application of Eq. (1). Further studies are needed to determine this relative size and depth effect on the dominant mode of vibration.

Consistency of the Air-Coupled IE Method

Acoustic scan tests were repeated three times along Row E, which represents the deck centerline, in the simulated bridge sample to study the consistency of the test method. Figs. 7(a and b) show repeated spectral B-scan images (frequency versus spatial location) from the air-coupled IE data using Prototypes A and B, respectively. The spectral amplitude is indicated by contour plots, where dark areas represent high amplitude. The test results show reasonably good consistency over the scanned area. In particular, the low-frequency indications associated with shallow Delamination Defects DL2, DL3, and DL6 are consistently seen. However, the responses at higher frequencies (greater than 5 kHz) are less consistent, with more apparent signal noise present.

Temperature Maps from Infrared Tests

Three representative thermograms taken of the sample and remapped into plan view are shown in Fig. 8. In Fig. 8(a) results 45 min after sunrise are shown, in which the overnight cooling effect is observed. The range of temperatures reported in this image is only about 6°C (11°F). Nevertheless, the presence of delamination is indicated as local cool regions that can be clearly differentiated from the surrounding solid concrete. The location and size of shallow Delaminations DL1−DL6 are accurately identified, regardless of the defect areal size. Some indication of the presence of deep Delamination D7 is also seen in the image. However, deep Delamination D8 and shallow Delamination D9 are not readily seen in the image; these results agree with the frequency maps from the air-coupled IE data. The fact that shallow Delamination DL9 is not indicated strengthens the contention that this particular defect may suffer from fabrication errors or be comprised of inappropriate material to simulate delamination for IR and IE tests. In addition, the IR images are also effective in distinguishing the severity of the delaminations (i.e., widths of the delamination itself). Defects DL4, DL5, and DL6 show a greater

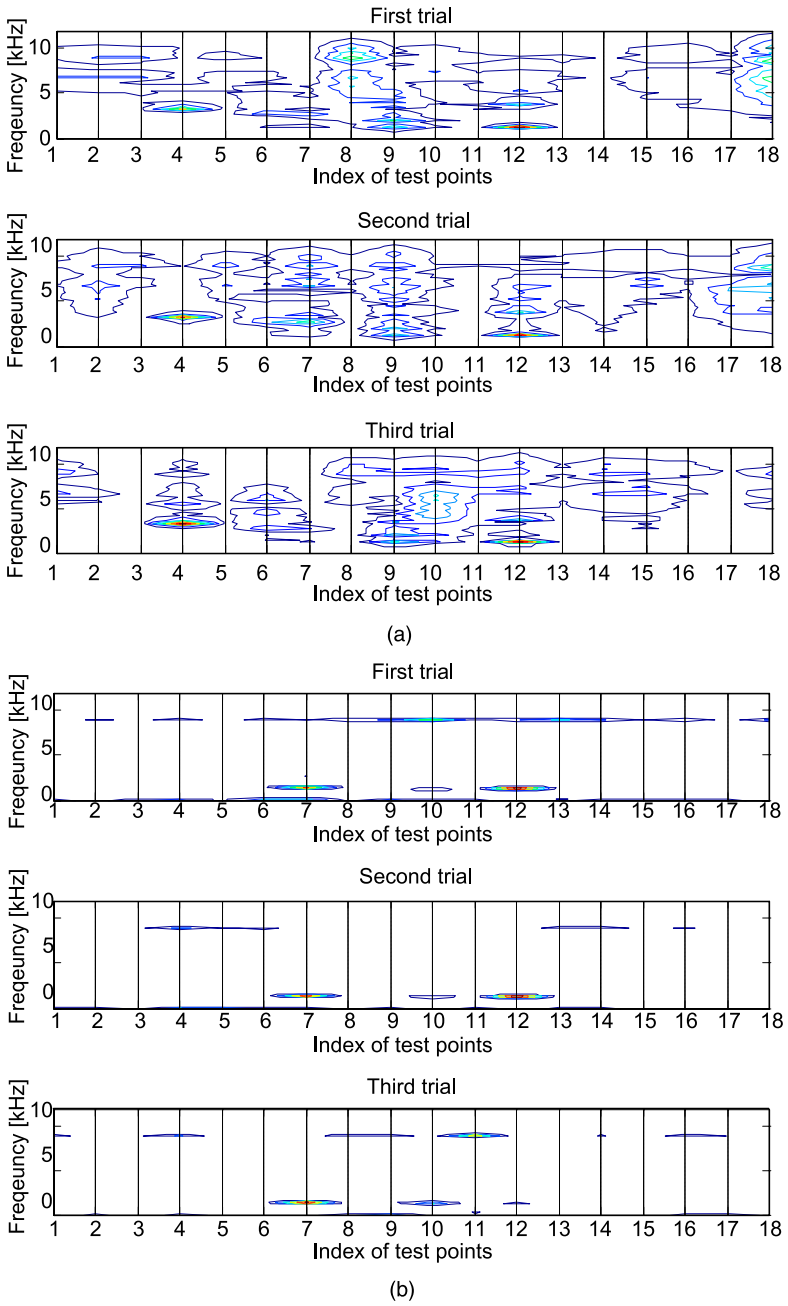

Fig. 7. Repeated spectral B-scan plots along Test Line D for the full length of the fabricated test slab using the (a) IE testing equipment of Prototype A and (b) IE testing equipment of Prototype B (shaded contour lines indicated peaks in amplitude spectra)

temperature contrast with the surrounding material than the other defects. These particular defects were simulated with thicker pieces of foam (see Table 1), and thus acted as better thermal insulators, restricting heat flow into or out of the slab. Consequently, the delaminations with larger widths (i.e., more severe ones) acted as better thermal insulators and resulted in higher temperature contrast on the surface.

Fig. 8(b) is a thermogram of the same surface taken 3 h 45 min after sunrise. Here, the temperature range within the image is 14°C (25°F), much larger than in Fig. 8(a). Despite the large temperature range, this image shows no indication of any delamination whatsoever; only the influence of the surface paint on the emissivity of the concrete is apparent. This behavior illustrates a limitation of passive IR thermography; i.e., the performance of the method depends on ambient environmental conditions. The reason for this is that the temperature contrast shifts through equilibrium between the cooling effect overnight and the heating effect of the sun during the day. Thus, the sense of the thermogram reverses when the heating effect becomes dominant. This is illustrated in Fig. 8(c), taken 7 h 45 min after sunrise. Here, the image temperature range reduces to about 5°C (7°F). The thermogram again accurately indicates shallow Delaminations DL1−DL6; this time as light spots. DL9 remains undetected. The deep delaminations are not revealed; therefore, 7 h of heating appears to be insufficient in contrast to the 15 h of nightly cooling. These results show that the successful use of the IR thermography depends on appropriate weather conditions and on being able to collect data at the right point in time of the day/night cycle. In addition, data interpretation can be complicated by local variations in surface properties (emissivity) that depend on roughness or

J. Bridge Eng. 2012.17:928-939.

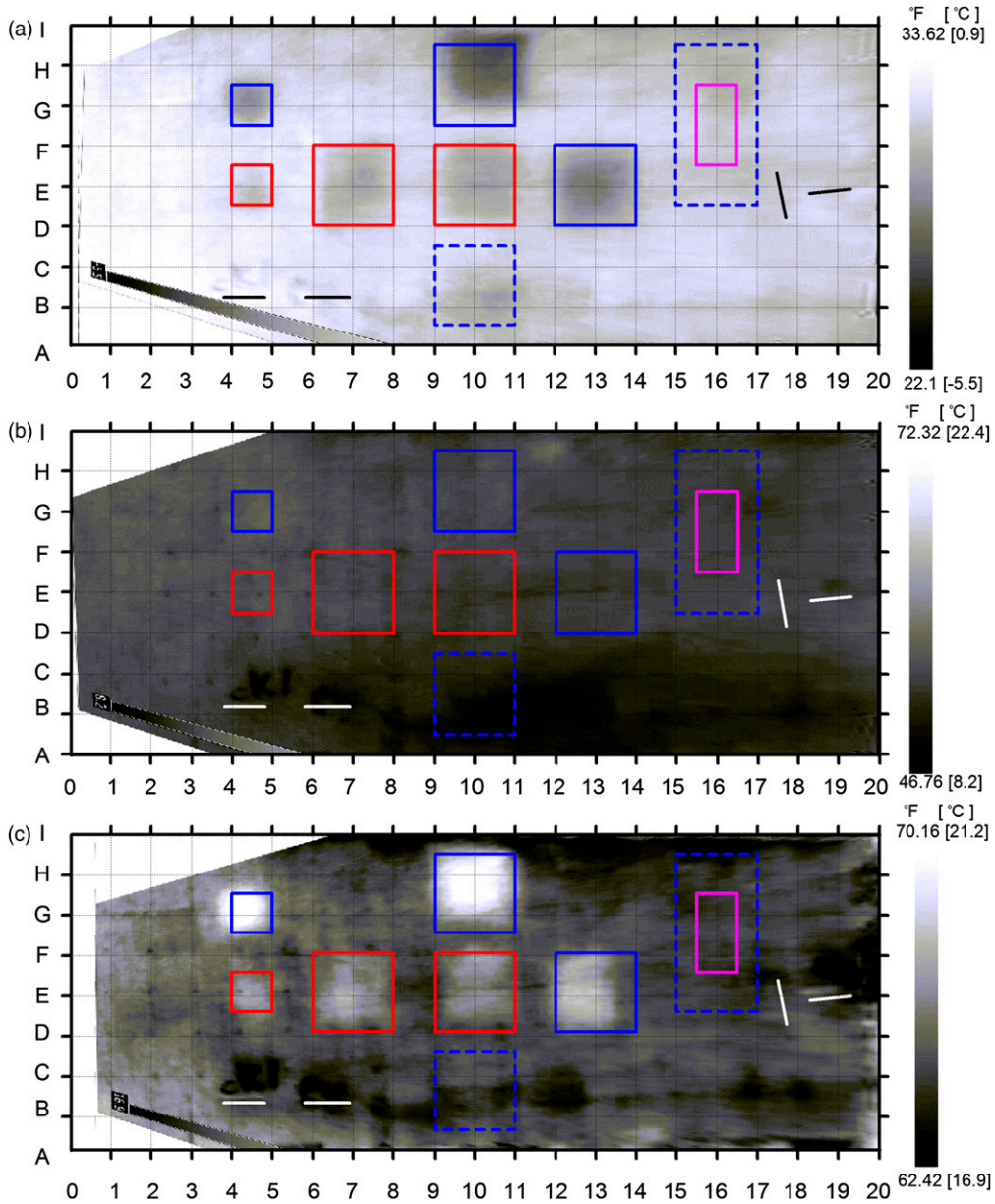

Fig. 8. IR images taken from the concrete specimen in various environmental conditions: (a) 3/4 h after sunrise, $T = 3.2°C$ (37.8°F), Rh = 44%; (b) 3 3/4 h after sunrise, $T = 17.2°C$ (63°F), Rh = 22%; (c) 7 3/4 h after sunrise, $T = 17.7°C$ (64°F), Rh = 21%

inhomogeneity of the concrete surface and paint or patching on the concrete surface [Fig. 8(b)]. Finally, the range and sense of the temperature within the thermograms varied with the ambient condition, which limited the ability to set fixed rule-based criteria to interpret the images. Despite these limitations, IR thermography can accurately define the location and extent of the shallow delamination under appropriate testing conditions. Furthermore, the optical nature of the method enables fast and efficient first screening of large concrete bridge decks. One of the more interesting results of this study is that thermograms obtained using the nightly cooling effect [Fig. 6(a)] can reveal both shallow and deep delaminations more clearly than those obtained from the heating effect from the sun [Fig. 6(c)] as proposed in ASTM D4788 (ASTM 1997).

Fusion of IE and IR Data

Based on the presented air-coupled IE and passive IR thermography results, a simple data fusion technique is proposed that builds on the advantages of each method. For this purpose the most reliable results were extracted from frequency maps and thermograms, using distinct rule-based criteria for each, and then fused into a single image.

The air-coupled IE frequency maps shown in Figs. 6(a and b) were converted to binary images with 400 by 1,000 pixel dimension, where a peak frequency of less than 6 kHz is reported as black and otherwise as white. Consequently, the resulting binary images corresponding to frequency maps in Figs. 6(a and b) are shown in Figs. 9(a and b), which effectively indicate the locations of all shallow delamination defects (except DL9) for both prototypes using a simple consistent rule-based criterion. The location of deep Delamination DL7 is indicated in Fig. 9(a) (Prototype A) but not in Fig 9(b) (Prototype B) because of the spatial testing resolution limits. However, the areal sizes of the defects in these IE binary images are underestimated in each case. This could be explained by the following two causes: (1) the limited spatial resolution of the IE tests in this study and (2) the rough edges of delamination defects

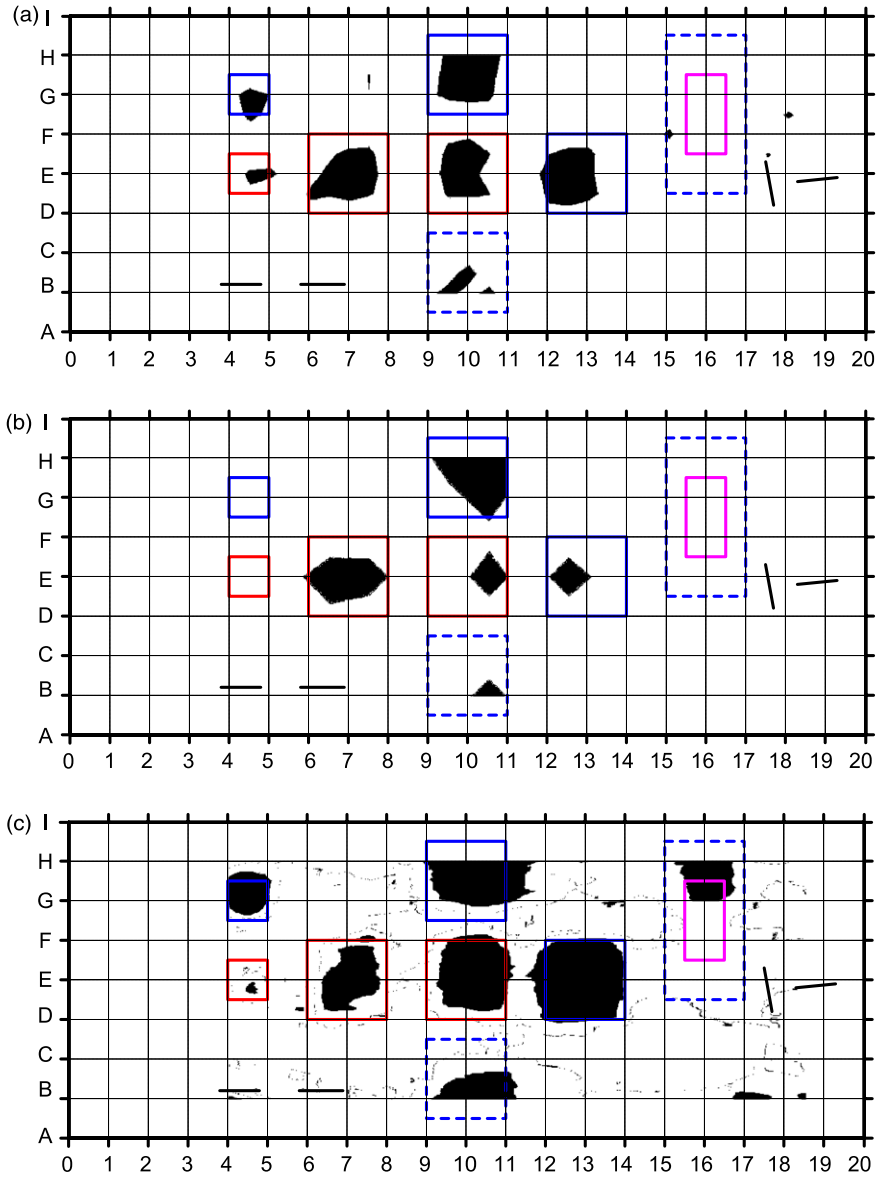

Fig. 9. Binary images presenting the predicted locations of defects from the IE frequency maps shown in (a) Fig. 6(a) and (b) Fig. 6(b) and (c) from the cooling effect IR image shown in Fig. 8(a) (shading indicates the expected defect region determined by each method)

simulated by the foam pieces, which may generate wave scattering—type attenuation, especially for a wave-based method.

The IR thermogram data obtained from the overnight cooling effect [shown in Fig. 8(a)] were converted to a binary image using rule-based criteria, temperatures below the 80th percentile of the full temperature range are presented as black and all other temperatures as white; this image is shown in Fig. 9(c). Compared with the images from the IE [Figs. 9(a and b)], the binary image from IR thermography [Fig. 9(c)] more effectively indicates the areal extent of the shallow delamination defects. Also, in Fig. 9(c), an indication of the presence of deep Delamination DL8 is seen, which was not seen in any other test result. The image also contains small anomalous indications across the entire surface, which appear as thin lines running across the surface. These false indications are likely a result of surface emissivity variations on the concrete. However, it is difficult to find general rule-based criteria for interpretation of quasi-passive IR thermography because of the variable nature of the data in terms of both temperature range and sensitivity.

Finally, the three binary images of the air-coupled IE and IR thermography were combined into a new fused image. First, the detected delamination defect locations were extracted from the air-coupled IE data. In the first fused image, the two binary images in Figs. 9(a and b) were combined into one image [shown in Fig. 10(a)]. The centroid location for each of the indicated delamination regions was calculated using the image processing toolbox in *MATLAB*; the centroid locations are indicated by asterisks in Fig. 10(a). The areal extents of the delamination region were obtained from the IR binary image in Fig. 9(c). The surface emissivity noise seen in the binary image in Fig. 9(c) was removed by implementing the following rule-based criteria: (1) detected regions whose areal size was less than 65 pixels (i.e., 25 cm^2) were excluded and (2) a centroid located more than 50 pixels (i.e., 31 cm) from any centroid of major delaminations detected by the IE [see Fig. 10(a)] was excluded. This IE-IR fused image [shown in Fig. 10(b)], accurately defines the location and areal extents of all the shallow delaminations, without anomalous surface emissivity noise indications. Thus, the simple noise suppression

J. Bridge Eng. 2012.17:928-939.

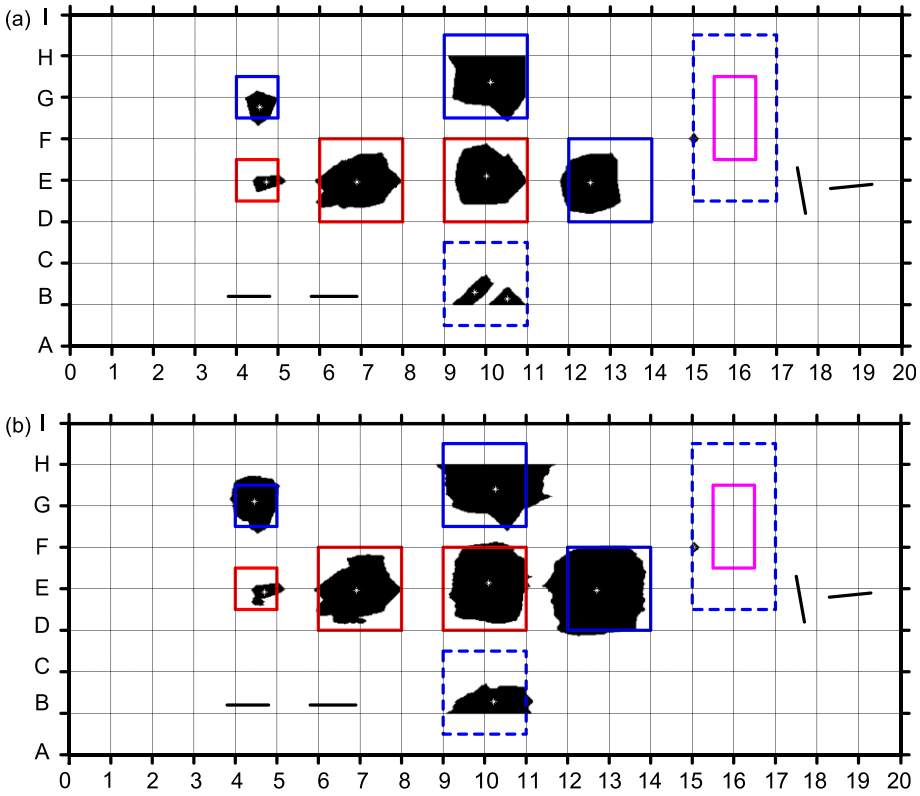

Fig. 10. Fused image presenting the locations of defects from both (a) air-coupled IE testing systems and (b) air-coupled IE testing and IR thermography (the location of the centroid is presented as asterisks)

algorithm was effective in improving the correlation between the fused image and the designed location of delamination. The multiple test fusion method in this study is similar to that proposed by previous researchers for characterizing bridge deck corrosion using a wide range of tests (Huston et al. 2011). In this study, the writers focused on only two of the more promising NDT methods (i.e., IE and IR methods) specifically for delamination damage in RC bridge decks and directly verified the performance in terms of delamination detection.

The results in this study demonstrate that fusion of IE and IR data enables consistent, practical, and sensitive detection of shallow delamination defects in concrete. Rule-based criteria can be applied to IE data, collected from a sufficiently spaced test grid, to identify the location of defects. Then, IR data, collected under ideal ambient conditions, can more accurately define the areal extent and shape of the defects at each of the indicated locations. However, more studies are needed to improve the effectiveness of data fusion, which may include (1) developing improved NDT methods to maximize advantages in individual methods and (2) improving signal processing techniques for individual data results and the fused data.

Conclusions

Based on the results presented in this paper, the following conclusions are drawn:

1. The noncontact nature of air-coupled IE enables efficient acoustic scanning of large concrete structures, which significantly improves testing speed. Generally, consistency of the method is reasonably good especially for frequencies below 5 kHz. Frequency maps built up from acoustically scanned data demonstrate that air-coupled IE is very effective in detecting shallow delamination defects, assuming the spatial resolution of the testing grid is sufficiently small. The location of the delaminations can be defined using rule-based criteria for the data: any peak response less than 6 kHz is indicated as a shallow delamination defect at that point.
2. It was difficult to clearly identify deep delaminations using air-coupled IE data in this study. In some cases a deep delamination is indicated by an increase in peak frequency; this appears to be the case for deep delaminations with larger areal size and only when IE data from a microphone with a broad frequency range (4−80 kHz at ± 2 dB), such as that in Prototype B, is used. In other cases the deep delamination is indicated by regions of slightly lower peak frequency; this appears to be the case for deep delaminations with smaller areal extent, although some deep delaminations were not detected with this criterion.
3. The spatial resolution of the IE testing grid is important: finer testing grids enable detection of delaminations with smaller areal size. In general, delamination defects smaller (in lateral dimension) than twice the test spacing are difficult to detect. Furthermore, the areal size of the defect is not accurately determined from IE data peak frequency maps because of limited spatial testing resolution and the nature of the flexural mode of vibration.
4. Quasi-passive IR thermography detects all shallow delamination defects when optimal testing and ambient environmental conditions prevail. Under good ambient conditions the areal extent of shallow delamination defects are well defined. One of the most interesting results of this study is that the overnight cooling effect can be used to detect both shallow and deep delaminations, providing clearer images than using the morning heating effect; a more detailed analysis of this behavior is currently being carried out by the writers. Nevertheless,

J. Bridge Eng. 2012.17:928-939.

rule-based criteria are difficult to employ with IR data because of the variable nature of the data in terms of both temperature range and sense.

5. The fusion of IE and IR data enables consistent, practical, and sensitive detection of shallow delaminations. Rule-based criteria can be applied to IE data collected from a sufficiently spaced test grid to identify the location of defects. Then, IR data collected under ideal ambient conditions can determine the areal extent and shape of the defects at each of the indicated locations.

Acknowledgments

The writers acknowledge Dr. Kerry Hall, Mr. Suyun Ham, and Mr. Xiaowei Dai for their valuable assistance with the experiments, and Dr. Soheil Nazarian from the University of Texas at El Paso for preparation of the experimental specimen. Also, the writers are grateful for support provided through the SHRP II project program under the direction of Dr. Nenad Gucunski from Rutgers University.

References

American Concrete Institute (ACI). (1998). "Nondestructive test methods for evaluation of concrete in structures." *Rep. ACI 228.2R-98*, ACI, Farmington Hills, MI.

ASTM. (1997). "Standard test method for detecting delaminations in bridge decks using infrared thermography." *D4788-97*, West Conshohocken, PA.

Cheng, C.-C., and Sansalone, M. (1995a). "Determining the minimum crack width that can be detected using the impact-echo method. Part 1: Experimental study." *Mater. Struct.*, 28(2), 74−82.

Cheng, C.-C., and Sansalone, M. (1995b). "Determining the minimum crack width that can be detected using the impact-echo method. Part 2: Numerical fracture analyses." *Mater. Struct.*, 28(3), 125−132.

FLIR Systems. (2011). "FLIR T400 technical specifications." 〈http://www.flir.com/uploadedFiles/Thermography_APAC/Products/Product_Literture/T400_Datasheet%20APAC(1).pdf〉 (Aug. 9, 2012).

Geyer, E., and Arndt, D. (1993). "Merkblatt für thermografische untersuchungen an bauteilen und bauwerken." *Merkblatt B 5*, Deutsche Gesellschaft für Zerstörungsfreie Prüfung e.V. DGZfP, Fachausschuss Zerstörungsfreie Prüfung im Bauwesen, Unterausschuss Optische und Thermografische Verfahren, Berlin.

Gibson, A., and Popovics, J. S. (2005). "Lamb wave basis for impact-echo method analysis." *J. Eng. Mech.*, 131(4), 438−443.

Holland, S. D., and Chimenti, D. E. (2003). "Air-coupled acoustic imaging with zero-group-velocity Lamb modes." *Appl. Phys. Lett.*, 83(13), 2704−2706.

Huston, D., Cui, J., Burns, D., and Hurley, D. (2011). "Concrete bridge deck condition assessment with automated multisensor techniques." *Struct. Infrastruct. Eng.*, 7(7-8), 613−623.

In, C. W., Kim, J. Y., Kurtis, K. E., and Jacobs, L. J. (2009). "Characterization of ultrasonic Rayleigh surface waves in asphaltic concrete." *NDT Int.*, 42(7), 610−617.

Kee, S.-H. (2011). "Evaluation of crack-depth in concrete using non-contact surface wave transmission measurement." Ph.D. dissertation, Univ. of Texas−Austin, Austin, TX.

Kee, S. H., and Zhu, J. (2010). "Using air-coupled sensors to determine the depth of a surface-breaking crack in concrete." *J. Acoust. Soc. Am.*, 127(3), 1279−1287.

Koch, G. H., Brongers, M. P. H., Thompson, N. G., Virmani, Y. P., and Payer, J. H. (2002). "Corrosion cost and preventive strategies in the United States." *Rep. No. FHWA-RD-01-156*, Dept. of Transportation, Federal Highway Administration, McLean, VA.

Maldague, X. (2001). "Infrared and thermal testing." *Nondestructive testing handbook*, American Society for Nondestructive Testing, Columbus, OH.

Moore, M., Phares, B., Graybeal, B., Rolander, D., and Washer, G. (2001). "Reliability of visual inspection for highway bridges: Volume I: Final report." *Rep. No. FHWA-RD-01-120*, Dept. of Transportation, Federal Highway Administration, McLean, VA.

Ryden, N., Lowe, M. J. S., and Cawley, P. (2008). "Non-contact surface wave scanning of pavements using a rolling microphone array." *Review of progresses in quantitative nondestructive evaluation*, D. O. Thompson and D. E. Chimenti, eds., Vols. 27A and 27B, American Institute of Physics, Melville, NY, 1328−1332.

Sansalone, M. (1996). "Impact-echo: The complete story." *ACI Struct. J.*, 94(71), 777−786.

Tawhed, W. F., and Gassman, S. L. (2002). "Damage assessment of concrete bridge decks using impact-echo method." *ACI Mater. J.*, 99(28), 273−281.

Tolstoy, I., and Usdin, E. (1953). "Dispersive properties of stratified elastic and liquid media: A ray theory." *Geophysics*, 18(4), 844−869.

Zhu, J., and Popovics, J. S. (2005). "Non-contact imaging for surface-opening cracks in concrete with air-coupled sensors." *Mater. Struct.*, 38(283), 801−806.

Zhu, J., and Popovics, J. S. (2007). "Imaging concrete structures using air-coupled impact-echo." *J. Eng. Mech.*, 133(6), 628−640.